

## **General Disclaimer**

### **One or more of the Following Statements may affect this Document**

- This document has been reproduced from the best copy furnished by the organizational source. It is being released in the interest of making available as much information as possible.
- This document may contain data, which exceeds the sheet parameters. It was furnished in this condition by the organizational source and is the best copy available.
- This document may contain tone-on-tone or color graphs, charts and/or pictures, which have been reproduced in black and white.
- This document is paginated as submitted by the original source.
- Portions of this document are not fully legible due to the historical nature of some of the material. However, it is the best reproduction available from the original submission.

**NASA TECHNICAL  
MEMORANDUM**

**NASA TM X-71787**

**NASA TM X-71787**

(NASA-TM-X-71787) AN EMPIRICAL MODEL FOR  
THE MIXING OF A ROW OF DILUTION JETS WITH A  
CONFINED CROSSFLOW (NASA) 18 p HC \$3.50

**N76-13429**

**CSCI 20D**

**G3/34**

**Unclas  
05625**

**AN EMPIRICAL MODEL FOR THE MIXING OF A ROW  
OF DILUTION JETS WITH A CONFINED CROSSFLOW**

by J. D. Holdeman  
Lewis Research Center  
Cleveland, Ohio 44135

and

R. E. Walker  
Aerojet Liquid Rocket Company  
Sacramento, California 95813



**TECHNICAL PAPER to be presented at Fourteenth Aerospace  
Sciences Meeting sponsored by the American Institute of  
Aeronautics and Astronautics  
Washington, D. C., January 26-28, 1976**

# AN EMPIRICAL MODEL FOR THE MIXING OF A ROW OF DILUTION JETS WITH A CONFINED CROSSFLOW

J. D. Holdeman\*

NASA-Lewis Research Center  
Cleveland, Ohio

and

R. E. Walker\*\*

Aerojet Liquid Rocket Company  
Sacramento, California

## Abstract

An empirical model has been developed for predicting the temperature distribution downstream of a row of cool jets injected normal to a hot confined crossflow. The model is based on the assumption that all properly non-dimensionalized vertical temperature profiles can be expressed in a self-similar form. The scaling parameters in this form have been correlated in terms of the independent flow and geometric variables. The effect of parametric variation of each of the independent variables on the experimental and predicted profiles are examined. The predicted distributions show excellent agreement with the data over a wide range of the independent variables.

## Introduction

The objective of this study was to model the penetration and mixing characteristics of multiple jets of cooling air injected normally into a heated crossflow in a constant area duct. The study was motivated by considerations of dilution zone mixing in gas turbine combustion chambers. For this application, rapid mixing of the diluent air with the hot combustion gases leaving the primary zone is desired to (1) provide a rapid quench for any continuing chemical reactions, (2) provide a suitable temperature distribution at the turbine inlet, and (3) reduce combustor length.

The experimental data on which the model is based were obtained by the Aerojet Liquid Rocket Company (ALRC) under NASA Contract NAS3-15703, and are reported in Refs. 1 and 2. The temperature field model was developed by ALRC under NASA Contract NAS3-18026 (Ref. 3). Data for selected tests from the Ref. 2 experiments have been used by Pratt & Whitney Aircraft to generate correlations to characterize the behavior of the dilution process (Ref. 4). The results of Refs. 3 and 4 are similar in that they both provide satisfactory profile predictions over the range of the data base used in Ref. 4. Because a larger data base was used in Ref.

3, these correlations can be used for a wider range of independent variables. Also, the correlations of Ref. 3 are somewhat less cumbersome than those in Ref. 4, and the relative importance of each of the independent variables in the correlations is more readily apparent. In this paper, the effect of parametric variation of each of the independent variables on both the experimental and predicted profiles (using the correlations of Ref. 3) are examined.

## The Data Base

A schematic of the multiple jet flow field with the principal flow and geometric variables identified appears in Fig. 1. The test section was 30.48 cm wide by 10.16 cm high. For all of the test results shown in this paper the nominal mainstream conditions were: velocity,  $U_{\infty} = 15$  m/sec; temperature,  $T_{\infty} = 600$  K. The jet velocity,  $V_j$ , was varied from 25 to 85 m/sec with the jets at ambient temperature,  $T_j = 300$  K. The jets entered the test section through sharp-edged orifices in the plate separating the main duct from the secondary air plenum chamber.

The test conditions were established with the jet-to-mainstream momentum flux ratio,  $J = (\rho_j V_j^2) / (\rho_{\infty} U_{\infty}^2)$ , and the jet-to-mainstream density ratio,  $\rho_j / \rho_{\infty}$ , as the primary independent flow variables. Momentum flux ratios investigated ranged from 6 to 60, with density ratios varied from 1.5 to 2.5. The symbols and parameters referenced in this paper are defined in Appendix A.

The primary independent geometric variables were the orifice size and spacing between adjacent orifices. These were expressed in dimensionless form as the ratio of the duct height to the orifice diameter,  $(4 \leq H/D \leq 16)$ , and the ratio of the orifice spacing to the orifice diameter,  $(2 \leq S/D \leq 6)$ . Although the experiments were performed with  $S/D$  and  $H/D$  as the independent geometric variables, the ratio of these,  $S/H$ , may be considered as an independent variable in the place of either  $S/D$  or  $H/D$ . The orifice area may be expressed in dimensionless form as  $A_j/A_{\infty} = (\pi/4) [(H/D)(S/D)]$  which is the orifice-to-mainstream area ratio. The orifice configurations investigated are shown in Fig. 2. The ratio of the jet flow to mainstream flow,  $\dot{w}_j/\dot{w}_{\infty}$ , can be expressed in terms of the independent flow and geometric

\*Aerospace Engineer, Combustion and Pollution Research Branch, Member AIAA.

\*\*Senior Engineer, Analytical Design, Member AIAA.

ORIGINAL PAGE IS  
OF POOR QUALITY

variables as

$$\frac{\dot{W}_1}{\dot{W}_\infty} = \left[ \sqrt{\frac{\rho_1}{\rho_\infty}} \sqrt{J} \frac{\pi}{4} C_d \right] / \left[ \left( \frac{H}{D} \right) \left( \frac{S}{D} \right) \right] \quad (1)$$

For this investigation, the orifice discharge coefficient,  $C_d$ , varied from 0.66 at the lowest momentum flux ratio to 0.62 at the highest momentum flux ratio.

Because the objective of the study was to identify orifice configurations appropriate for optimum mixing within a minimum combustor length, the downstream stations surveyed were defined in terms of the duct height,  $H$ . Measurements of total pressure and temperature were made at 20 vertical and 21 horizontal positions in each of five planes at downstream locations from  $X/H = 0.25$  to  $X/H = 2.0$ . The total span of the 21 horizontal positions was varied to correspond to twice the orifice spacing for each plate. This distance varied from 2.54 cm for the smallest orifice spacing to 20.32 cm for the largest spacing. The  $Z$  plane through the orifice center is defined as the centerplane ( $Z = 0$ ) and the  $Z$  plane midway between adjacent orifices is defined as the midplane ( $Z = S/2$ ). Thus the span of the measurements provided 4-fold data redundancy. Additional aspects of the experimental program and the facility used are discussed in Ref. 2.

The results for the temperature field are presented as vertical profiles of the dimensionless temperature difference ratio,  $\theta$ , where

$$\theta = \frac{T_{lc} - T}{T_\infty - T_j} \quad (2)$$

and  $T$  is the local total temperature,  $T_\infty$  is the total temperature of the undisturbed mainstream flow, and  $T_j$  is the jet total temperature. Because  $T_\infty > T_j$ , the largest values of  $\theta$  in any profile correspond to the coolest regions of the flow.

#### Flow Field Model

The empirical model for this three-dimensional shear flow is based on the observation that the properly non-dimensionalized vertical temperature profiles everywhere in the flow field can be expressed in the following self-similar form:

$$\frac{\theta - \theta_{\min}^\pm}{\theta_c - \theta_{\min}^\pm} = \exp \left[ - \ln 2 \left( \frac{\frac{Y - Y_c}{H}}{\frac{W_{1/2}^\pm}{H}} \right)^2 \right] \quad (3)$$

In this expression,  $\theta$  is the local temperature difference ratio given by Eq. (2), and  $\theta_c$ ,  $\theta_{\min}^\pm$ ,  $Y_c/H$ , and  $W_{1/2}^\pm/H$  are scaling parameters as shown in Fig. 3.  $\theta_c$  is the maximum temperature difference ratio in the vertical profile, and  $Y_c$  is its location. The line defined by the locus of  $Y_c$  as a function of downstream distance ( $X$ ) for  $Z = 0$  is the thermal trajectory (centerline).

Because the flow is confined and the profiles are not symmetric about the centerline, the half-widths ( $W_{1/2}^\pm$ ) and the minimum temperature difference ratios ( $\theta_{\min}^\pm$ ) are different for the + side ( $Y/H > Y_c/H$ ) and the - side ( $Y/H < Y_c/H$ ) of the profiles. Correlations have been developed for each of the scaling parameters in terms of the independent variables  $J$ ,  $S/D$ ,  $H/D$ ,  $X/H$ , and  $Z/S$ . The complete set of correlations are given in Appendix B. This is only one possible set of correlations; in Ref. 4, Cox gives another set which also yield satisfactory profile predictions. The primary differences between the results given here and those in Ref. 4 are (1) the forms of the present correlations are simpler than those of Ref. 4 and the relative importance of each of the independent variables is more readily apparent and (2) profiles can be predicted using the correlations in Appendix B over a wider range of the independent variables since the data base used in the present investigation was larger than the one used in Ref. 4. The main weakness of the present correlations is that their form precludes their use in predicting profiles for semi-confined flows (large  $H/D$  or large  $S/D$ ) or the single jet flow (large  $H/D$  and  $S/D$ ).

#### Results and Discussion

##### Effect of Downstream and Lateral Distance

The variation of the centerplane ( $Z = 0$ ) temperature profiles with downstream distance for both the smallest ( $J = 6$ ) and largest ( $J = 60$ ) momentum flux ratios tested are shown in Fig. 4 for an orifice configuration with  $S/D = 4$  and  $H/D = 8$ . For this geometry, the agreement between predicted and experimental profiles is slightly better at the low momentum flux ratio than at the high one. At the high momentum flux ratio, the jet penetration increases monotonically with increasing downstream distance. However, at the low momentum flux ratio, the penetration is non-monotonic, with a slight recurving toward the injection wall evident at the largest downstream distance. This effect appeared whenever the jet penetrated to less than half the duct height, and was particularly acute when a two-dimensional jet flow was established near the injection wall ( $Y = 0$ ). In Fig. 5, lateral profiles at  $X/H = 1$  are shown for the same conditions as in Fig. 4. For the low momentum flux ratio, the profiles vary substantially with lateral distance, and the model provides a satisfactory prediction of both the decrease in the maximum penetration and the decrease

in the maximum temperature difference with increasing distance from the centerplane. A thermal contour plot for this condition would show the traditional "kidney" shape resulting from the twin vortices, which develop with the flow from each jet. The lateral variation of the temperature profiles is small at the high momentum flux ratio, indicating that there is substantial interaction between adjacent jets, which tends to diffuse the vorticity. The result is a nearly plane flow as shown in Fig. 5(b).

#### Effect of Flow Variables

The jet-to-mainstream momentum flux ratio,  $J = (\rho_j V_j^2) / (\rho_\infty U_\infty^2)$ , was found to be the most important operating variable influencing the mixing. The magnitude of this effect on the centerplane ( $Z = 0$ ) profiles is shown in Fig. 6. These profiles are at a distance of one duct height downstream from the injection point for a geometry with  $S/D = 4$  and  $H/D = 12$ . The prediction of the centerplane profiles is good except that the side half-width is too large for low  $J$  values. It should be noted that the ratio of jet flow to mainstream flow increases by slightly more than a factor of three from  $J = 6$  to  $J = 60$ .

Although experiments were performed with the density ratio varied from 1.5 to 2.5 at constant momentum flux ratio, no consistent correlation with density ratio was found in the present investigation. Thus the density ratio does not appear in any of the correlations in Appendix B. This is not meant to imply that the mixing is independent of density ratio for all  $\rho_j/\rho_\infty$ , but rather indicates that, for the limited variation in the experiments ( $1.5 < \rho_j/\rho_\infty < 2.5$ ), the effect, if any, is of second order importance.

#### Effect of Geometric Variables

The momentum flux ratio, and the density ratio are dependent on the combustor design conditions, e.g., inlet temperature and pressure, reference velocity, pressure drop, and fuel-air ratio. Thus for a given combustor, the dilution zone design parameters which may be varied to influence the combustor exit temperature distribution are the orifice diameter, orifice spacing, and orifice shape. However, since the flow conditions for a given combustor determine the required orifice area, the orifice size and spacing must be correctly coupled. In Fig. 7, centerplane temperature profile data at  $X/H = 1$  for momentum flux ratios of 6 and 60 are shown for three orifice configurations all having orifice-to-mainstream area ratios of 0.049. The differences in the profiles are evident, indicating that for a given operating condition considerable variations in the downstream temperature distributions can be effected by changes in the orifice diameter and spacing. The most significant difference between the experimental and pre-

dicted profiles in Fig. 7 is for the largest orifices at the highest momentum flux ratio. These conditions cause flow impingement on the opposite wall, and the temperature distributions in the resultant strongly bifurcated flow do not conform to the self-similar profile shape assumed in the model. Thus, the lack of agreement between predicted and experimental profiles is not surprising.

The variations shown in Fig. 7 are consistent with the results of Ref. 5, where fewer large orifices were found to provide better jet penetration than a larger number of small orifices for the same orifice area. In the following paragraphs, the effects of parametric variation of the geometric variables at a constant momentum flux ratio of  $J = 25$  are discussed.

Effect of varying orifice spacing at constant orifice diameter ( $H/D = 8$ ,  $J = 25$ ,  $X/H = 1$ ) - For a given jet diameter, momentum flux ratio, and downstream distance the penetration of the dilution jets increases with increasing spacing as shown in the centerplane profiles in Fig. 8(a). Also, the maximum temperature difference in each profile decreases as would be expected since the ratio of jet flow to mainstream flow varies inversely with  $S/D$ . The agreement between experimental and predicted profiles is excellent in all cases. The variation of the corresponding midplane profiles is shown in Fig. 8(b). As spacing increases, the centerplane and midplane profiles differ as the flow develops three-dimensionally. The prediction of the midplane profiles is good, but of course there is some spacing for which further increases would have no effect on the experimental distributions. Beyond this spacing, the flow is semi-confined and the model (as presently formulated) is not appropriate.

Effect of varying orifice diameter at constant  $S/D$  ( $S/D = 2$ ,  $J = 25$ ) - For a given  $S/D$ , momentum flux ratio, and downstream distance, the jet penetration increases significantly with increasing orifice diameter (decreasing  $H/D$ ) as shown in the centerplane profiles at  $X/H = 1$  in Fig. 9. The maximum temperature difference in these profiles increases slightly as the ratio of jet flow to mainstream flow increases ( $\dot{w}_j/\dot{w}_\infty \sim 1/(H/D)$ ), but the primary effect is in the percentage of the span cooled by the dilution flow. The predicted and experimental profiles compare favorably except for the smallest orifice size where the model underpredicts the trajectory (too much recurving) and underpredicts the maximum temperature difference.

Some insight into the confining effect of the opposite wall is given by the centerplane profiles of  $\theta$  vs  $Y/D$  at constant  $X/D$  (Fig. 10). The maximum temperature difference decreases slightly with decreasing  $H/D$ , but the primary effect is the suppression of the jet penetration. The effects shown here are in agreement with the results of experiments on heated jets in a confined cross-flow reported in Ref. 6.



Effect of varying orifice diameter at constant spacing ( $S/H = 0.5$ ,  $J = 25$ ) - For a constant  $S/H$  (constant spacing), constant momentum flux ratio, and constant downstream distance, increasing the orifice diameter shifts the temperature profiles to higher  $\theta$  values consistent with the greater dilution airflow. Although the penetration of the jets also increases slightly, the shape of the temperature profiles is not altered appreciably. This effect is shown by the predicted and experimental centerplane profiles at  $X/H = 1$  and  $2$  in Fig. 11 for three orifice configurations with a constant  $S/H = 0.5$ , but with jet flow-to-mainstream flow ratios varying from  $0.11$  to  $0.46$ . The profiles shown in Figs. 8, 9, and 11 suggest that for  $J = 25$ , optimum mixing of the jets with the mainstream flow is achieved with  $S/H = 0.5$ . The profiles in Fig. 7 show that for  $J = 6$ , the best mixing was achieved with  $S/H = 1$ , and for  $J = 60$ , the best mixing was achieved with  $S/H = 0.25$ .

#### Application to Combustor Design

These results suggest that for a given momentum flux ratio and downstream distance, combustor design procedure should first identify the  $S/H$  value required to obtain the desired profile shape, and to position the profile at the desired spanwise location. The orifice size would then be chosen to provide the required jet-to-mainstream flow ratio. Because the penetration varies slightly with orifice size, adjustments (using the correlation relations in the flow model) would be necessary to arrive at the final dilution jet configuration. Although the geometries and test conditions of the experimental data base are representative of current design practice for annular gas turbine combustors, the flow model cannot completely describe dilution zone performance, since, as discussed by Cox in Ref. 4, the effects of liner cooling airflow, non-uniform dilution zone inlet temperature distribution, and flow area convergence in the dilution zone are not considered. Also, the experiments considered injection from one side toward an opposite wall, thus the results are applicable to one-side entry combustors or (since the wall may be considered to be a plane of symmetry as shown by the opposed jet and jet/wall data in Ref. 6) to dual-side entry combustors with directly opposed jets. At present there are no experimental data available that could be used to extend the model to dual-side, staggered jet dilution zone configurations.

#### Summary of Results

An empirical model is presented for predicting the temperature distribution downstream of a row of dilution jets injected normal to a hot confined crossflow. The model is based on the assumption that all properly non-dimensionalized vertical temperature profiles can be

expressed in a self-similar form. The scaling parameters in this form have been correlated in terms of the independent variables. These are the momentum flux ratio ( $6 < J < 60$ ), the ratio of the spacing between adjacent orifice to the orifice diameter ( $2 < S/D < 6$ ), the ratio of the duct height to the orifice diameter ( $4 < H/D < 16$ ), the dimensionless downstream distance ( $0.25 < X/H < 2$ ), and the dimensionless off-centerplane distance ( $0 < Z/S < 0.5$ ). Profiles predicted using the flow model are in excellent agreement with the experimental data except for combinations of the flow and geometric variables which result in strong jet impingement on the opposite wall.

The effects of parametric variation of the independent variables on the predicted and experimental profiles can be summarized as follows:

1. The momentum flux ratio was the most important flow variable influencing the penetrations and mixing. For the limited range of density ratios covered by the experiments, no correlation with density ratio was found.
2. For a given orifice diameter, increasing the spacing between adjacent jets increased the penetration and increased the uniformity of the vertical profiles. However, horizontal distributions became more non-uniform with increased spacing as the mixing became more three-dimensional.
3. For a constant spacing to diameter ratio ( $S/D$ ), penetration and mixing at any  $X/H$  increased with increasing jet diameter.
4. For a constant spacing ( $S/H$ ), increasing the orifice diameter increased the magnitude of the temperature difference ratios, and increased the penetration slightly, but the basic shape of the profiles was not altered appreciably.

#### Appendix A - Symbols

$A_j/A_\infty$	orifice area to mainstream area ratio, $= (\pi/4) [(H/D)(S/D)]$
$C_d$	orifice discharge coefficient
$D$	orifice diameter; see Fig. 1
$D_j$	jet diameter $= D \sqrt{C_d}$
$H$	duct height = 10.16 cm; see Fig. 1
$H/D$	duct height to orifice diameter ratio
$J$	momentum flux ratio, $= (\rho_j V_j^2) / (\rho_\infty U_\infty^2)$
$S$	spacing between centerlines of adjacent orifices; see Fig. 1
$S/D$	spacing to orifice diameter ratio
$S/H$	spacing to duct height ratio
$T$	temperature at any location in flow field
$T_j$	jet total temperature, = 300 K
$T_\infty$	mainstream total temperature, = 600 K

$U_{\infty}$	mainstream velocity, = 15 m/sec
$V_j$	jet velocity
$\dot{w}_j/\dot{w}_{\infty}$	jet-to-mainstream mass flow ratio
$X$	distance downstream from jet injection location; see Fig. 1
$X/H$	dimensionless downstream distance
$Y$	distance above injection plane; see Fig. 1
$Y/H$	dimensionless vertical distance
$Z$	off-centerplane distance; see Fig. 1
$\theta$	dimensionless temperature difference ratio, = $(T_{\infty} - T)/(T_{\infty} - T_j)$
$\rho_j$	jet density
$\rho_{\infty}$	mainstream density

#### Appendix B - Correlations

The temperature difference ratio,  $\theta$ , at any point in the flow field is determined from:

$$\theta = \theta_{\min}^{\pm} + (\theta_c - \theta_{\min}^{\pm}) \exp \left[ - \ln 2 \left( \frac{\frac{Y - Y_c}{H} - \frac{Y_c}{H}}{\frac{W_{1/2}^{\pm}}{H}} \right)^2 \right] \quad (B1)$$

The correlations for the scaling parameters in this expression are given in this appendix. In the correlations, a second subscript has been appended to each of the parameters to denote the transverse ( $Z$ ) location for which the expression is appropriate. The scaling parameters are defined for planes from  $Z = 0$  (centerplane) to  $Z = S/2$  (midplane). In the correlations,  $D_j$ , the jet diameter, is used in place of  $D$ , the orifice diameter, where  $D_j = D \sqrt{C_d}$ . For the range of conditions tested in this study,  $0.62 < C_d < 0.66$ .

#### Correlations for Predicting the Centerplane Temperature Profiles

##### Thermal trajectory (centerline)

$$\frac{Y_{c,o}}{H} = 0.539 J^{0.25} \left( \frac{S}{D_j} \right)^{0.14} \left( \frac{H}{D_j} \right)^{-0.45} \left( \frac{X}{H} \right)^{0.17} e^{-b} \quad (B2)$$

where

$$b = \left[ 0.09 \left( \frac{X}{H} \right)^2 \left( \frac{H}{S} - \frac{\sqrt{J}}{3.5} \right) \right]$$

The exponential term is required to suppress the predicted penetration when the main flow is blocked by the

establishment of a two-dimensional wall jet flow.

##### Centerline temperature difference ratio

$$\theta_{c,o} = \theta_{EB} + (1 - \theta_{EB}) \left[ 1.536 J^{-0.35} \left( \frac{X}{D_j} \right) \right]^f \quad (B3)$$

where

$$f = 1.15 \sqrt{\frac{S}{H} / \left( 1 + \frac{S}{H} \right)}$$

and

$$\theta_{EB} = 1 / \left[ 1 + \frac{4}{\pi} \left( \frac{S}{D_j} \right) \left( \frac{H}{D_j} \right) \right]$$

$\theta_{EB}$  is the temperature difference ratio which would result from complete mixing of the jet and mainstream flows, and thus represents the asymptotic condition for the  $\theta_{c,o}$  decay. The decay exponent,  $f$ , varies from 0.38 to 0.81 for the conditions tested in this study. The data of Ref. 6, which were for heated jets in a confined crossflow show a similar  $\theta_{c,o}$  decay characteristic. In Ref. 7, a decay exponent of 0.63 was found appropriate for a single jet injected perpendicular to a semi-infinite crossflow. For a round jet in a coflowing stream, an exponent of 0.67 would be expected.

##### Minimum centerplane temperature difference ratios

$$\theta_{\min,o}^+ = \theta_{c,o} (1 - e^{-c^+}) \quad (B4)$$

where

$$c^+ = 0.038 J^{1.62} \left( \frac{S}{D_j} \right)^{1.5} \left( \frac{H}{D_j} \right)^{-2.6} \left( \frac{X}{H} \right)^{1.1}$$

$$\theta_{\min,o}^- = \theta_{c,o} (1 - e^{-c^-}) \quad (B5)$$

where

$$c^- = 1.57 J^{-0.3} \left( \frac{S}{D_j} \right)^{-1.4} \left( \frac{H}{D_j} \right)^{0.9} \left( \frac{X}{H} \right)^{0.9}$$

##### Centerplane half-widths

$$\frac{W_{1/2,o}^+}{H} = 0.162 J^{0.18} \left( \frac{S}{D_j} \right)^{-0.25} \left( \frac{X}{H} \right)^{0.5} \quad (B6)$$

$$\frac{W_{1/2,o}^-}{H} = 0.20 J^{0.15} \left( \frac{S}{D_j} \right)^{0.27} \left( \frac{H}{D_j} \right)^{-0.38} \left( \frac{X}{H} \right)^{0.12} \quad (B7)$$

Note that in this investigation the jet half-widths are defined as the vertical distance from the centerline to where  $\theta = (\theta_{c,o} + \theta_{\min,o}^{\pm})/2$ .

Caution should be exercised in comparing the apparent profile widths directly with the half-width correlation relations, since the apparent widths of the profiles depend on  $W_{1/2,o}^{\pm}$ ,  $\theta_{\min,o}^{\pm}$ , and  $\theta_{c,o}$ .

#### Correlations for Predicting the Off-Centerplane Variation of the Temperature Profile Scaling Parameters

##### Off-centerplane penetration

$$\frac{Y_{c,z}}{H} - \frac{Y_{c,o}}{H} \left[ 1 - \left( \frac{Z}{S/2} \right)^2 e^{-g} \right] \quad (B8)$$

where

$$g = 0.227 J^{0.67} \left( \frac{S}{D_i} \right)^{-1} \left( \frac{X}{D_i} \right)^{0.54}$$

##### Off-centerplane maximum temperature difference ratio

$$\theta_{c,z} = \theta_{c,o} \left[ 1 - \left( \frac{Z}{S/2} \right)^2 e^{-d} \right] \quad (B9)$$

where

$$d = 0.452 J^{0.53} \left( \frac{S}{D_i} \right)^{-1.53} \left( \frac{X}{D_i} \right)^{0.83}$$

##### Off-centerplane minimum temperature difference ratios and half-widths

$$\theta_{\min,z}^{\pm} = \theta_{\min,o}^{\pm} \left( \frac{\theta_{c,z}}{\theta_{c,o}} \right) \quad (B10)$$

$$\frac{W_{1/2,z}^{\pm}}{H} = \frac{W_{1/2,o}^{\pm}}{H} \quad (B11)$$

Equations (B10) and (B11) represent major simplifying assumptions which were justified by the agreement obtained between predicted and experimental profiles.

#### References

1. Holdeman, J. D., Walker, R. E., and Kors, D. L., "Mixing of Multiple Dilution Jets with a Hot Primary Airstream for Gas Turbine Combustors," AIAA Paper 73-1249, Las Vegas, Nev., 1973.
2. Walker, R. E. and Kors, D. L., "Multiple Jet Study," June 1973 Aerojet Liquid Rocket Co., Sacramento, Calif.; also NASA CR-121217.
3. Walker, R. E. and Eberhardt, R. G., "Multiple Jet Study Data Correlations," Apr. 1975, Aerojet Liquid Rocket Co., Sacramento, Calif.; also NASA CR-134795.
4. Cox, G. B., Jr., "Multiple Jet Correlations for Gas Turbine Engine Combustor Design," ASME Paper 75-GT-45, Houston, Tex., 1975.
5. Norgren, C. T. and Humenik, F. M., "Dilution Jet Mixing Study for Gas-Turbine Combustors," TN D-4695, Aug. 1968, NASA.
6. Kamotani, Y. and Greber, I., "Experiments on Confined Turbulent Jets in Cross Flow," CR-2392, Mar. 1974, NASA.
7. Holdeman, J. D., "Correlations for Temperature Profiles in the Plane of Symmetry Downstream of a Jet Injected Normal to a Crossflow," TN D-6966, Sept. 1972, NASA.

ORIGINAL PAGE IS  
OF POOR QUALITY



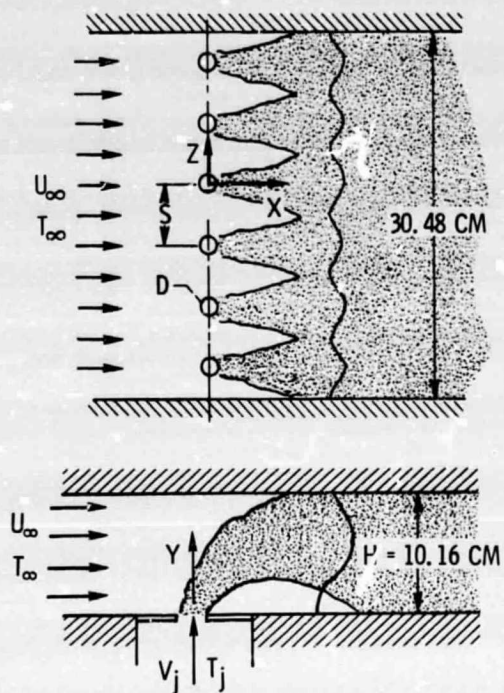


Figure 1. - Schematic of multiple jet flow.

PRECEDING PAGE BLANK NOT FILMED

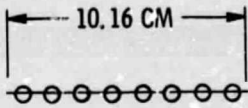
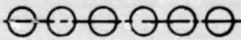
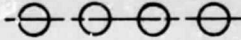
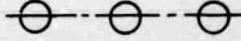
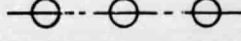
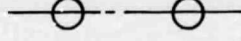

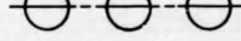
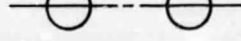
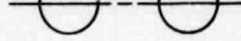
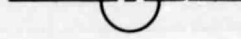
S/D	H/D	$A_j/A_\infty^*$	
2	16	0.025	
2	12	.033	
2	8	.049	
3	8	.033	
4	12	.016	
4	8	.025	
6	8	.016	
2	6	.065	
2.83	5.66	.049	
2	4	.098	
4	4	.049	

Figure 2. - Orifice plate configurations;  
 $*A_j/A_\infty = (\pi/4)/(H/D)/(S/D)$

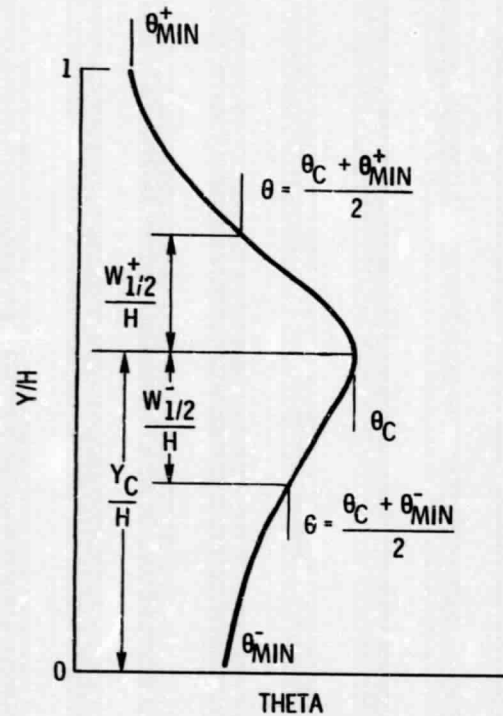


Figure 3 - Schematic of typical vertical temperature profile showing scaling parameters.

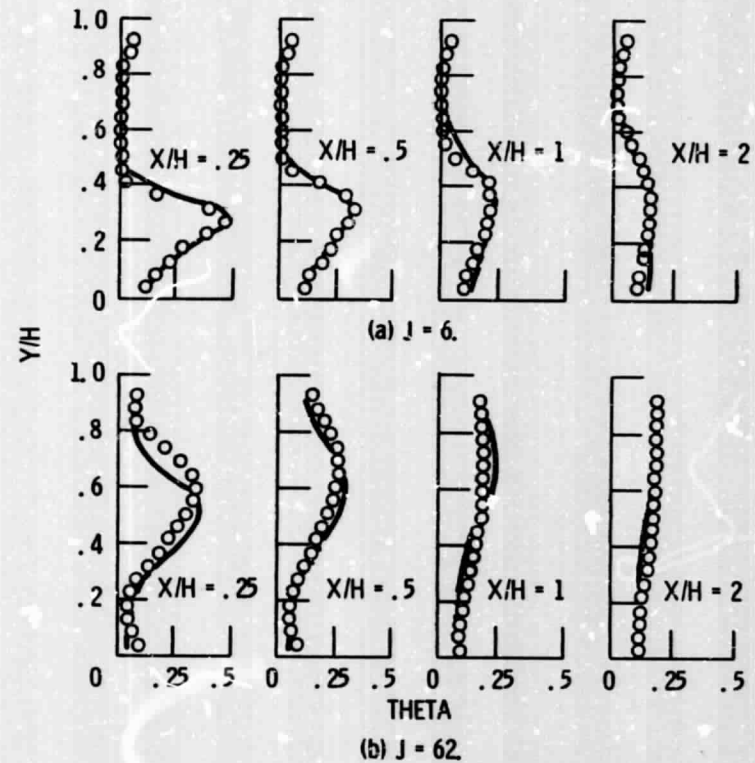


Figure 4 - Variation of centerplane temperature profiles with downstream distance;  $S/D = 4$ ,  $H/D = 8$ .

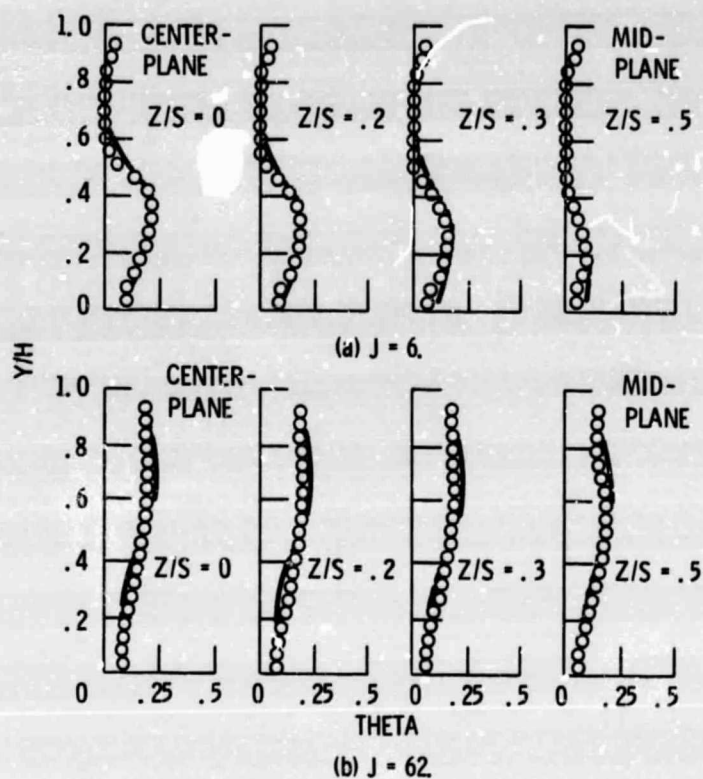


Figure 5. - Variation of temperature profiles with distance from centerplane;  $X/H = 1$ ,  $S/D = 4$ ,  $H/D = 8$ .

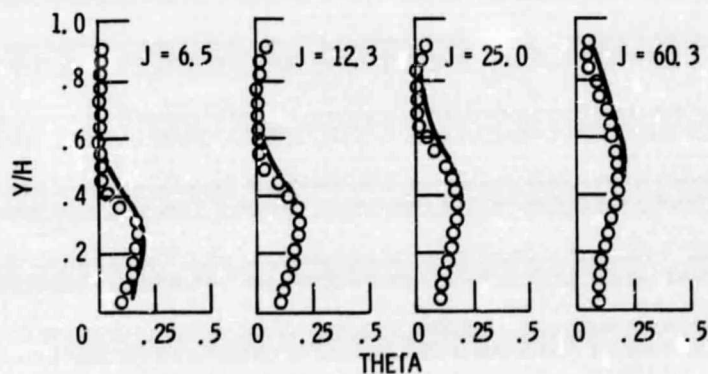


Figure 6. - Effect of momentum flux ratio on centerplane temperature profiles;  $X/H = 1$ ,  $S/D = 4$ ,  $H/D = 12$ .



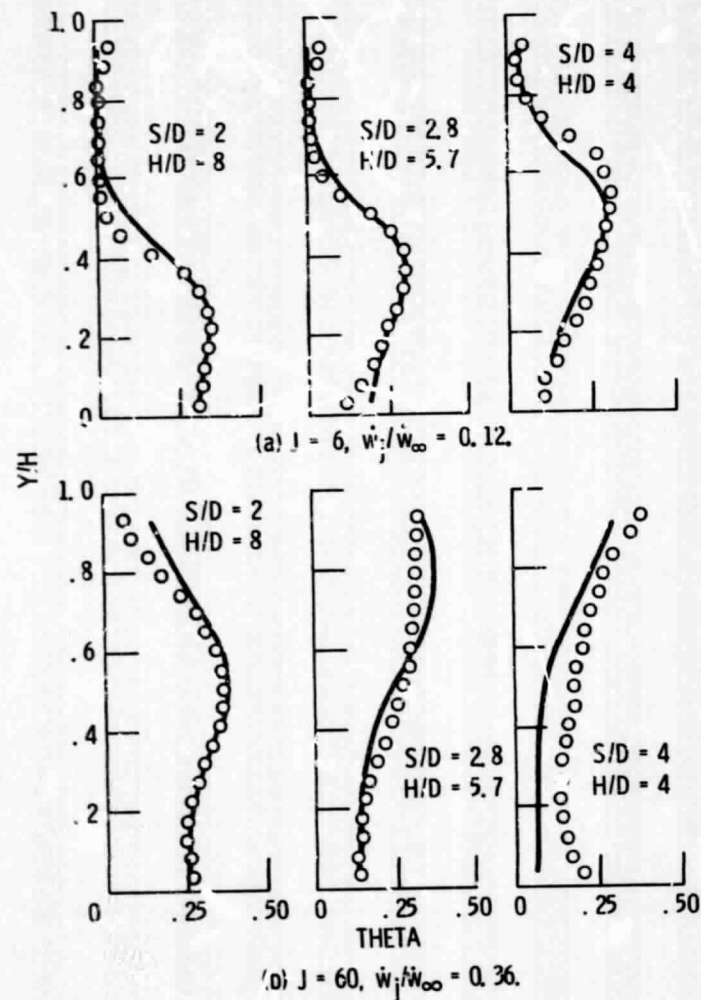


Figure 7. - Effect of geometric variables on centerplane temperature profiles at constant orifice area;  $A_j/A_\infty = 0.049$ .

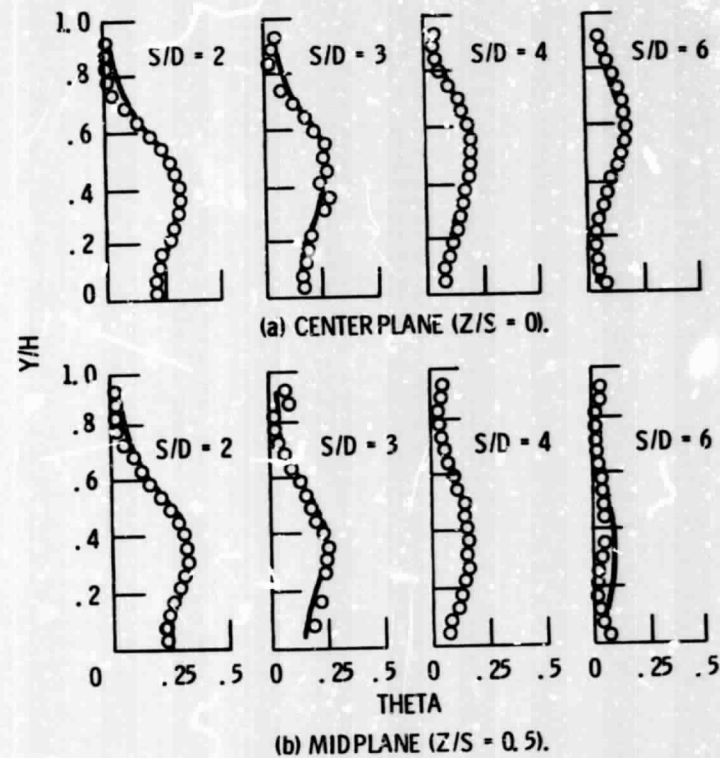


Figure 8. - Effect of varying spacing on temperature profiles for constant orifice diameter;  $H/D = 8$ ,  $X/H = 1$ ,  $J = 25$ .

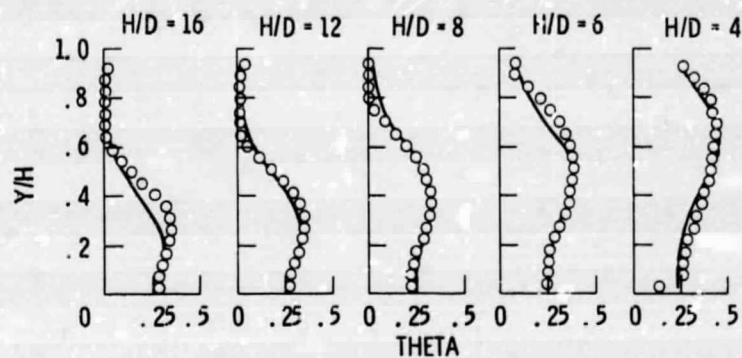


Figure 9. - Effect of varying orifice diameter on centerplane temperature profiles at constant  $S/D$ ;  $S/D = 2$ ,  $X/H = 1$ ,  $J = 25$ .

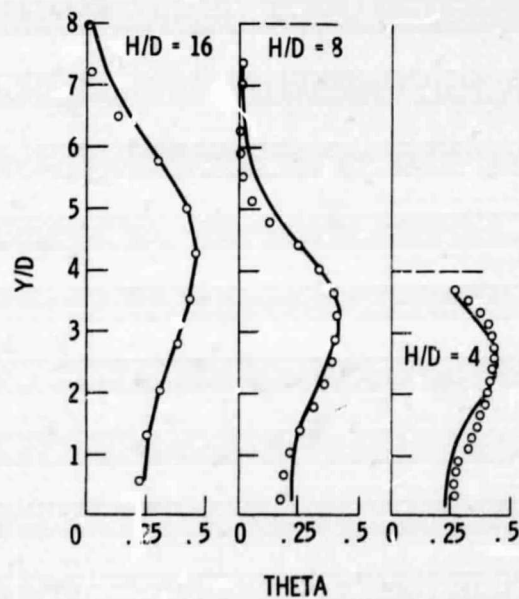


Figure 10. - Effect of confinement by the opposite wall on centerplane temperature profiles at constant  $S/D$ ;  $S/D = 2$ ,  $X/D = 4$ ,  $J = 25$ .

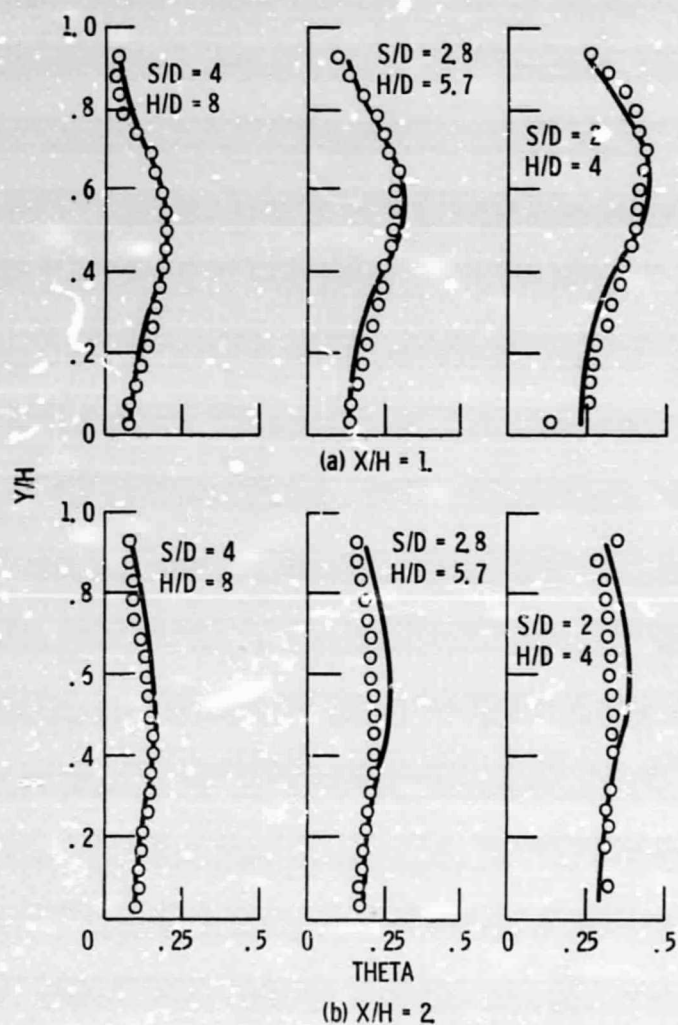


Figure 11. - Effect of varying orifice diameter on centerplane temperature profiles at constant  $S/H$ ;  $S/H = .5$ ,  $X/H = 1$ ,  $J = 25$ .